Phys Chem Minerals (1996) 23: 186–192

ORIGINAL PAPER

Th. Barkmann · L. Cemič

Impedance spectroscopy and defect chemistry of fayalite

Received June 29, 1995/Revised, accepted September 25, 1995

Abstract Impedance spectra of polycrystalline synthetic fayalite were measured at 900 °C and 1 atm pressure in a CO/CO_2 gas mixing furnace at oxygen fugacities $f_{O_2}=10^{-13}$ to 10^{-17} atm. The frequency range applied to the samples was 20 Hz–1 MHz. The spectra show two semicircular arcs, which are attributed to polarization processes within the bulk material and at the sample-electrode interface. Two different types of behaviour of the bulk resistance as a function of oxygen fugacity were observed. The first is proportional to the $-1/4.5$ to $-1/6$ power of f_{O_2}, which is consistent with the existing defect model. The second shows a lesser dependence on f_{O_2}, often lowered by a factor of about two, relative to the expected value, resulting in a resistance proportional to the $-1/10$ to $-1/12$ power of f_{O_2}. It is assumed, that the lesser f_{O_2}-dependence is caused by aliovalent impurities, producing an f_{O_2}-independent amount of charge carriers. The electrode arcs show a resistance proportional to the $-1/2$ to $-1/4$ power of oxygen fugacity, implying that a reaction with the gas phase is involved in the polarization process at the sample-electrode interface.

Introduction

All kinds of transport related properties of minerals, i.e. electrical conductivity, rheology, diffusion phenomena etc., depend on their defect chemistry. The concentration of point defects is controlled by the conditions of thermodynamic equilibrium. Therefore, the defect chemistry of minerals can be investigated by measurements of point defect concentrations under defined thermodynamic conditions, for the case of an ideal solution behaviour at low defect concentrations.

The electrical conductivity of minerals is determined by the concentration, charge and mobility of the point defects. The olivine endmember fayalite (Fe_2SiO_4) shows electronic p-type conduction via small polaron hopping (e.g. Sockel 1974), while in forsterite (Mg_2SiO_4) ionic contributions are also significant (e.g. Schock et al. 1989). Since the mobility of electronic charge carriers at constant temperature is 10^2–10^3 times higher than the mobility of ionic defects, the electrical properties of Mg, Fe-olivine solid solutions are controlled by the fayalite component. Hence, this study focuses on the investigation of the electrical properties of synthetic endmember fayalite. While there are numerous measurements of electrical conductivity of natural olivines (e.g. Wanamaker and Duba 1993; Schock et al. 1989), investigations on synthetic samples are scarce (e.g. Cemič et al. 1980). To the best of our knowledge, the only measurements of electrical conductivity of fayalite, performed under variable oxygen fugacities at 1 atm, are those of Sockel (1974). The author collected his data on polycrystalline samples, with an alternating current of fixed frequency (1.5 kHz) and by the use of Pt-electrodes (two-electrode arrangement). The investigated temperature range extended from 1000–1150 °C. The oxygen fugacity was controlled by a $CO-CO_2$ atmosphere. The use of a fixed frequency and Pt-electrodes can lead to experimental problems which complicate the data interpretation. The different polarization processes occurring in the sample-electrode system, i.e. bulk polarization as well as polarization at grain boundaries and the sample-electrode interface, have to be taken into account.

An important aspect of the present study is the application of impedance spectroscopy for the evaluation of the electrical properties of minerals. While this technique has been used for many years in solid state chemistry and physics, as well as materials science (introduced into solid state science by Cole and Cole 1941), up to now there exist only very few investigations in mineralogy (e.g. Roberts and Tyburczy 1993; Huebner and Dillenburg 1995; Nover et al. 1992). From impedance spectroscopic data, the contributions of the different polarization processes to the overall conductivity can be

Th. Barkmann (✉) · L. Cemič
Mineralogisch-Petrographisches Institut der Universität Kiel, Olshausenstraße 40–60, D-24098 Kiel, Germany

evaluated. It is, therefore, an appropriate method to deduce bulk conductivities from data of polycrystalline material, especially when two-electrode arrangements are used.

Impedance spectroscopy

Impedance spectroscopy involves the measurement of the complex quantity Z* (impedance) of a sample as a function of angular frequency ω. A sinusoidal signal U(ω) is defined by:

$$U(\omega)=U_0 \cdot \sin(\omega t) \quad (1)$$

where U_0=voltage, ω=angular frequency ($\omega=2\pi f$, f=frequency).

Application of the sinusoidal signal to a system will cause the flow of an alternating current of amplitude I, that is shifted in phase ϕ relative to the applied signal, where:

$$I(\omega)=I_0 \cdot \sin(\omega t+\phi) \quad (2)$$

The complex impedance Z* follows from Ohms law:

$$Z^*(\omega)=\frac{U^*(\omega)}{I^*(\omega)}=Z_0 \cdot e^{i\phi}$$

$$=Z_0 \cos\phi+iZ_0 \sin\phi=Z'+iZ'' \quad (3)$$

where

$$Z'=Z_0 \cos\phi \quad (4)$$

and

$$Z''=Z_0 \sin\phi \quad (5)$$

with Z′ and Z″ as the real and imaginary parts of the complex quantity Z*, and Z_0=magnitude of Z* and $i=\sqrt{-1}$. Therefore, a measurement of magnitude Z_0 and phase ϕ allows the calculation of the real and imaginary part, which are plotted against each other in the impedance spectra (Bode plot) as a function of frequency.

An ideal spectrum of a polycrystalline sample consists of 3 semicircular arcs, each representing a different polarization process occurring in the sample-electrode system, i.e. bulk, grain boundary and double layer polarization. The physical explanation of this behaviour is non trivial in many cases. Each polarization process can be treated as a result of capacitive and Ohmic properties. The spectra can be simulated by equivalent circuits as known from network theory. An ideal semicircular arc with the high frequency end passing through the origin can be modelled by a parallel RC circuit. Connecting three parallel RC circuits in series leads to the spectrum shown in Fig. 1. Ideal behaviour of a system is seldom. Depression of an arc, as shown in Fig. 2, is often observed. The usual way to model these data is by the use of

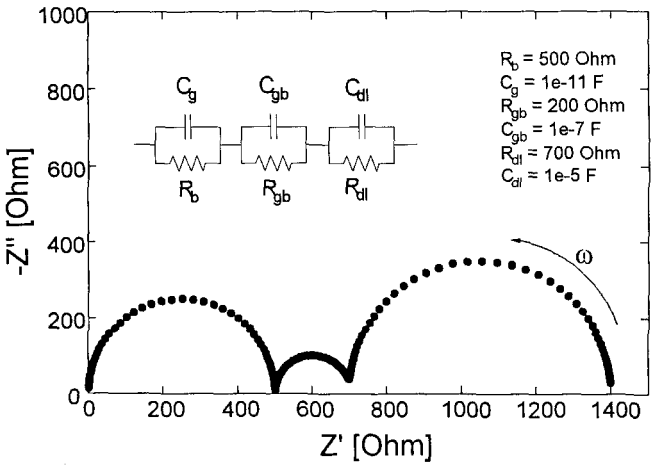

Fig. 1 Simulated ideal impedance spectrum of a polycrystalline sample, showing three polarization processes; R_b=bulk resistance, C_g=geometric capacity; R_{gb}=grain boundary resistance, C_{gb}=grain boundary capacity; R_{dl}=double layer resistance, C_{dl}=double layer capacity, ω=angular frequency

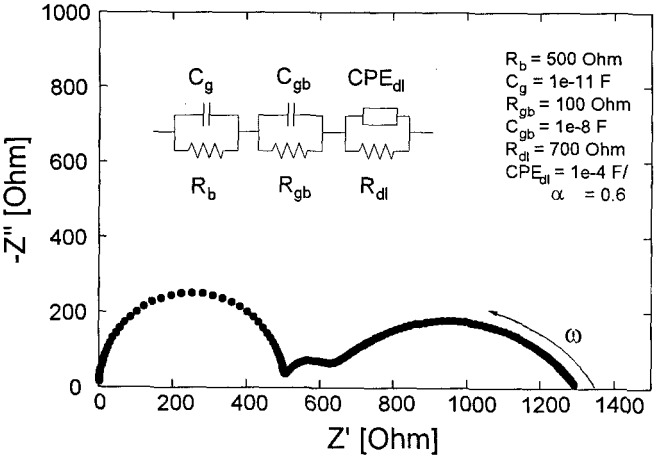

Fig. 2 Simulated impedance spectrum of a polycrystalline sample with a non-ideal (α=0.6) behaviour of the double layer capacitor ($\alpha_{ideal}=1$), leading to a constant phase element (CPE)

constant phase elements, CPE, which take into account the non-ideal behaviour of the capacitor in the circuit. The non-ideality is expressed by a variable, α, varying between 1 and 0. For α=1, the CPE becomes an ideal capacitor, for α=0 an ideal resistor (see e.g. Macdonald 1987; Roberts and Tyburczy 1993). By measuring a frequency spectrum over a wide range, e.g. 10^1–10^6 Hz, the different polarization processes in the sample-electrode system can be resolved, if the relaxation times τ_i ($\tau_i=R_iC_i$) of the processes differ by at least two or three orders of magnitude from each other.

Sample preparation and experimental procedure

The oxides Fe_2O_3 (99,999%, Aldrich Chemical Comp.) SiO_2 (p.a., Merck, Art. 657) and Fe (p.a., Merck, Art. 3819) were intensively mixed in stoichiometric fayalite composition and pressed to pel-

lets, then heated at 800–1100°C for 48–288 h in evacuated SiO_2-glass tubes. The oxygen fugacity was controlled by the Fe/FeO buffer during synthesis. The products were examined by X-ray diffraction, optical microscopy and microprobe analysis. Only polycrystalline fayalite without any detectable impurity phases was used for further experiments.

For measurements, in which the activity of SiO_2 should be unity, 1–3 wt.% excess-SiO_2 was added to a ground fayalite powder and an additional sintering was performed. The grain size varied between 20 and 2000 μm, depending on sintering time and temperature. The sintered products showed only closed porosity in optical and SEM investigations. Therefore, it is assumed that more than 90–92% of the theoretical density was obtained. Most of the sintered pellets were cut into rectangular bars (4.0×1.5×1.5 mm). In order to correlate the impedance arcs with the different polarization processes, the sample shape was also varied.

All measurements were performed in a vertical tube furnace. The oxygen fugacity was controlled by CO/CO_2 gas-mixtures and measured with a CSZ- (calcia-stabilized zirconia) sensor. The IW-buffer was used as an internal oxygen potential reference. The sensor was checked with bracketing experiments on the Fe/FeO and Ni/NiO equilibria by placing pellets of Fe or Ni adjacent to the sensor tip and varying the CO/CO_2-ratio. The oxygen fugacity was kept constant within $+/-0.1$ $\log f_{O_2}$ units over several weeks. The temperature was constant within $+/-1$ K on a vertical length of 40 mm. No horizontal temperature gradient was observed. A non-inductive winding and an additional steel cylinder served as induction shield in the electrical conductivity measurements. Electrodes were made of $Ag_{70}Pd_{30}$ alloys, while electrode leads were made of the same alloy or Pt. Because of the symmetrical arrangement and temperature homogeneity (<1 K) in the hot zone, no thermo-EMF was produced by the use of Pt leads. Impedance measurements were performed using a Hewlett Packard 4284 A LCR meter between 20 Hz and 1 MHz (two-electrode configuration). Only a small voltage of 20 mV was applied. All data were collected on a personal computer via an IEEE-bus.

The electrode problem

One of the most serious problems in electrical conductivity measurements of Fe-bearing samples at high temperatures and reducing conditions is the choice of an appropriate electrode material. Iron-loss to the electrodes leads to steadily increasing resistance and irreproducible data when Pt or Ir is used as electrode material. Huebner and Dillenburg (1995) observed a progressive increase with time in the double layer resistance of synthetic olivine (Synfo 85, T=1050°C, $\log f_{O_2} = -13.0$). They attributed the process to a steady loss of Pt-coating, that initially provided good contact to the sample. Wanamaker and Duba (1993) assigned a similar increase in resistance of San Carlos Olivine to iron-loss into the iridium electrodes they used. Iron-loss increases with iron content of the sample, temperature and decreasing oxygen fugacity. Hence, the electrical conductivity measurement of fayalite is a non-trivial problem, because of its high iron content and the extension of its T-f_{O_2} stability field towards reducing conditions (QFI).

Figure 3 shows the steady increase of the low frequency arc with time, measured on a sample of polycrystalline fayalite with Pt-electrodes (T=900°C, $\log f_{O_2} = -15.43$). In agreement with Wanamaker and Duba (1993), this work attributes the steady, irreversible increase of the double layer resistance to a major iron-loss

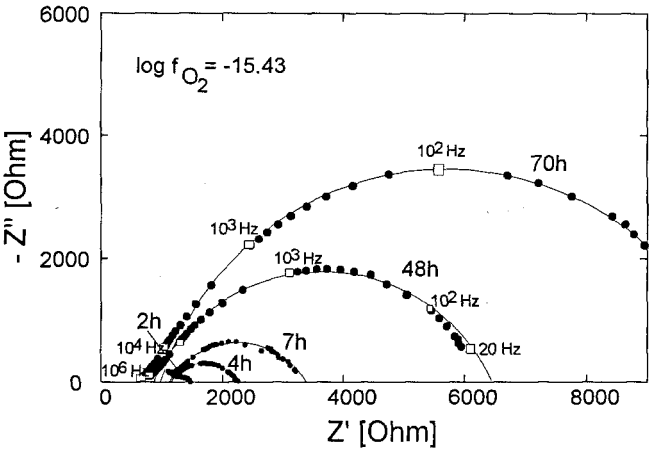

Fig. 3 Impedance spectrum of polycrystalline fayalite, showing steady increase of the low frequency arc (double layer polarization) due to iron loss of the sample to the Pt-electrodes; T=900°C, $\log f_{O_2} = -15.43$)

into the Pt-electrodes, leaving a steadily growing, highly resistive iron depleted zone between electrodes and non-altered sample material. Microprobe measurements and SEM investigations revealed SiO_2 precipitates on the fayalite sample surface. A presaturation of Pt with Fe does not solve the problem, because the activity of Fe in a PtFe alloy is f_{O_2}-dependent. Hence, Pt is not suitable as an electrode material for the measurement of iron bearing materials at high temperatures (i.e. >700°C) and reducing conditions (i.e. below QFM).

The only noble metal which does not strongly alloy with Fe is Ag. However, Ag cannot normally be used because of its low melting point (~960°C) and relatively high vapour pressure at temperatures well below its melting point. Ceramic electrodes, e.g. La-Cr-perovskites, are not conducting enough relative to fayalite, so that their own f_{O_2}-dependence of conductivity is not negligible. In this study, iron-loss was minimized by using $Ag_{70}Pd_{30}$ alloys. The disadvantages of this material are its relatively low melting point (~1150°C), fixing the maximum working temperature to ~1000°C, and the loss of small amounts of Pd to the sample, especially under strongly reducing conditions (i.e. below the IW-buffer). On the other hand, diffusion of small amounts of Pd into the outermost 50–100 μm of the sample provides good electrical contact.

Point defect thermodynamics of fayalite

A commonly accepted point defect model of fayalite was proposed by Nakamura and Schmalzried (1983) from thermogravimetric data, collected at 1130°C. They assumed ferric iron on regular sites, $Fe_{Fe}^{\cdot}$, vacancies in the iron sublattice, V_{Fe}'', and ferric iron on the silicon site, Fe_{Si}', as the majority defects. The defect notation follows Kröger and Vink (1956). Because of its high mobility, the electron hole associated with $Fe_{Fe}^{\cdot}$ is assumed to be

the main charge carrier in fayalite. According to Nakamura and Schmalzried (1983), the most probable reactions which lead to the formation of majority defects can be written:

$$1/2\ O_2(g)+Fe^x_{Fe}+Si^x_{Si}+1/2\ Fe_2SiO_4 = Fe'_{Si}+Fe^{\cdot}_{Fe}+3/2\ SiO_2 \quad (6)$$

$$6\ Fe^x_{Fe}+SiO_2+O_2(g)=2\ V''_{Fe}+4\ Fe^{\cdot}_{Fe}+Fe_2SiO_4 \quad (7)$$

The formation of the majority defects causes nonstoichiometry in fayalite. The defect concentration is related to the component activities and the oxygen fugacity through the mass action law of the defect reactions (6) and (7), giving:

$$[Fe'_{Si}]\cdot[Fe^{\cdot}_{Fe}]=K_6\cdot f_{O_2}\cdot a^{-3/2}_{SiO_2} \quad (8)$$

$$[V''_{Fe}]^2\cdot[Fe^{\cdot}_{Fe}]^4=K_7\cdot f_{O_2}\cdot a_{SiO_2} \quad (9)$$

where [ ] designates the site fraction of a defect species on its sublattice.

Due to strong coulombic interactions, association of defects may occur. The experimental data from Nakamura and Schmalzried (1983) indicate complete association of $[Fe'_{Si}]$ and $[Fe^{\cdot}_{Fe}]$ through the reaction

$$[Fe'_{Si}]+[Fe^{\cdot}_{Fe}]=\{Fe'_{Si}Fe^{\cdot}_{Fe}\} \quad (10)$$

Taking into account the electroneutrality condition

$$[V''_{Fe}]\approx 1/2\ (Fe^{\cdot}_{Fe}] \quad (11)$$

the authors deduced a stability field of fayalite as a function of oxygen fugacity and nonstoichiometry. According to the ideal anion/cation and cation/cation ratio in fayalite, they defined the nonstoichiometry in terms of the variables $\bar{\eta}$ and $\bar{\xi}$:

$$\bar{\eta}=\frac{n_O}{n_{Si}+n_{Fe}}-\frac{4}{3}=\frac{4}{3-2[V''_{Fe}]}-\frac{4}{3}=\frac{8}{9}[V''_{Fe}] \quad (12)$$

which is proportional to f_{O_2} (n designates the mole number), and

$$\bar{\xi}=\frac{n_{Si}}{n_{Si}+n_{Fe}}-\frac{1}{3}=\frac{1-[Fe'_{Si}]}{3-2[V''_{Fe}]}-\frac{1}{3}$$

$$=\frac{2}{9}[V''_{Fe}]-\frac{1}{3}[Fe'_{Si}Fe^{\cdot}_{Fe}] \quad (13)$$

leading to Fe-excess for $\bar{\xi}<0$ and Si-excess for $\bar{\xi}>0$.

Nakamura and Schmalzried (1983) deduced the equilibrium constants for the reactions (6) and (7) from thermogravimetric measurements. Simons (1984) studied the temperature dependence of K_7 (K_3 in the work of Nakamura and Schmalzried 1983) by EMF-measurements. He obtained:

$$\log K_7=-2.794-6376/T(K) \quad (14)$$

which agrees well with the value given by Nakamura and Schmalzried (1983). The other equilibrium constants

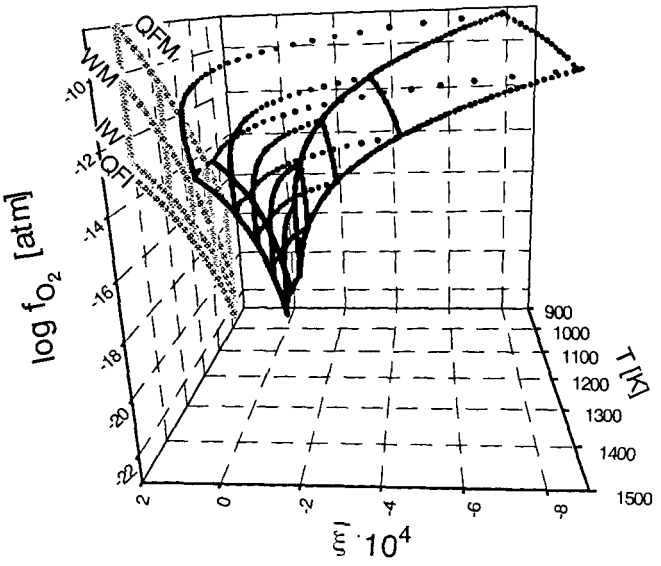

Fig. 4 Stability volume of fayalite as a function of temperature, oxygen fugacity and nonstoichiometry $\bar{\xi}$ ($\bar{\xi}<0$ means Fe-excess, $\bar{\xi}>0$ means Si-excess), calculated with equilibrium constants given in Nakamura and Schmalzried (1983) and Simons (1986). For the purpose of orientation, QFM-, QFI-, WM- and IW-buffer curves are shown as projections onto the T-f_{O_2} plane

were found to be independent of temperature by both Simons (1986) and Nakamura and Schmalzried (1983). With these data, the stability volume of fayalite as a function of oxygen fugacity, temperature and nonstoichiometry can be calculated (Fig. 4). As shown in Fig. 4, at higher temperatures fayalite is able to dissolve higher defect concentrations, before exsolution processes occur at the univariant phase boundaries. For better orientation in the T-f_{O_2}-$\bar{\xi}$ space, the QFM-, QFI-, MW- and IW-buffer curves are also shown as projections onto the T-f_{O_2} plane.

All measurements in this study were performed at 900°C. Figure 5 shows the stability field of fayalite as a function of oxygen fugacity and nonstoichiometry at this temperature, calculated with the equilibrium constants given by Nakamura and Schmalzried (1983) and Simons (1986). At the invariant points QFM and QFI, fayalite coexists with magnetite and SiO_2 or iron and SiO_2, respectively. Application of the mass action law to the corresponding defect reaction (7) leads to

$$K_7=\frac{[V''_{Fe}]^2\cdot[Fe^{\cdot}_{Fe}]^4}{a_{SiO_2}\cdot f_{O_2}} \quad (15)$$

and taking into account the electroneutrality condition (11):

$$[Fe^{\cdot}_{Fe}]=(4\cdot K_7)^{1/6}\cdot a^{1/6}_{SiO_2}\cdot f^{1/6}_{O_2} \quad (16)$$

Along the univariant phase boundary Fe_2SiO_4/SiO_2, the activity of SiO_2 in fayalite is fixed to one. Therefore, at constant temperature and fixed $a_{SiO_2}=1$, the impedance (or electrical conductivity) should vary to the sixth root of oxygen fugacity.

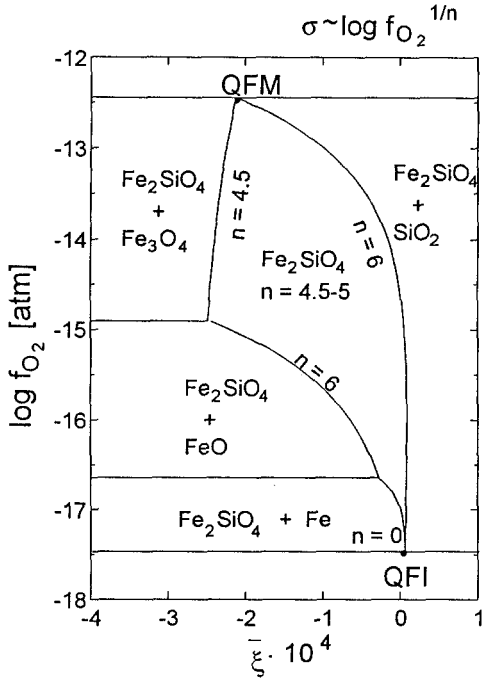

Fig. 5 Stability field of fayalite as a function of oxygen fugacity and nonstoichiometry at 900°C, calculated with equilibrium constants given in Nakamura and Schmalzried (1983) and Simons (1986)

Nakamura and Schmalzried (1983) defined a characteristic number, n, by:

$$\frac{\partial \log [\text{defect}]}{\partial \log f_{O_2}} = \frac{1}{n} \tag{17}$$

Hence, along the phase boundary Fe_2SiO_4/SiO_2, n equals 6. Analogous treatment of the other phase boundaries leads to n=4.5 (Fe_2SiO_4/Fe_3O_4), n=6 (Fe_2SiO_4/FeO) and n=0 (Fe_2SiO_4/Fe), as shown in Fig. 5. Within the stability field, i.e. without a coexisting binary oxide, n should vary between 4.5 and 5, depending on the nonstoichiometry of fayalite.

Results and analysis

Figure 6 shows a typical impedance spectrum of polycrystalline fayalite, covering the frequency range 20 Hz–1 MHz, measured at 900°C and $\log f_{O_2} = -16.10$. The spectrum shows two well resolved semicircular arcs. The bulk arc is covered only in its low frequency range, while the lower frequency arc is complete but slightly depressed. The first arc is attributed to bulk polarization, the second to a polarization process at the sample electrode interface. No grain boundary polarization was observed. All spectra were fitted with a non linear least-squares fitting program (Boukamp 1989). The fitted spectrum is in excellent agreement with the measured data. Because this study only focuses on relative variations of impedance, no geometric corrections with respect to sample shape were made.

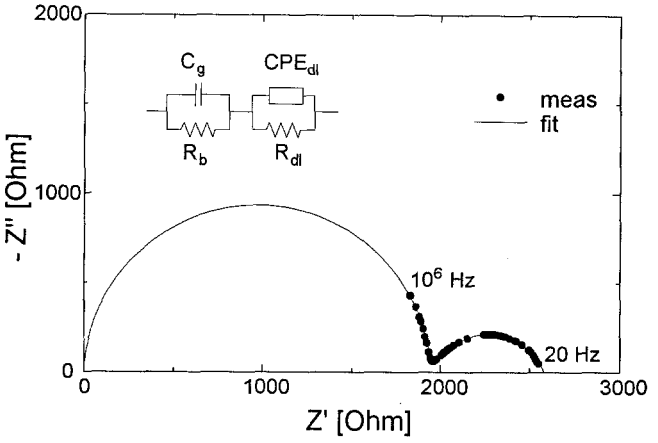

Fig. 6 Impedance spectrum of polycrystalline fayalite, measured from 20 Hz–1 MHz, 10 points per decade; T=900°C, $\log f_{O_2} = -16.10$

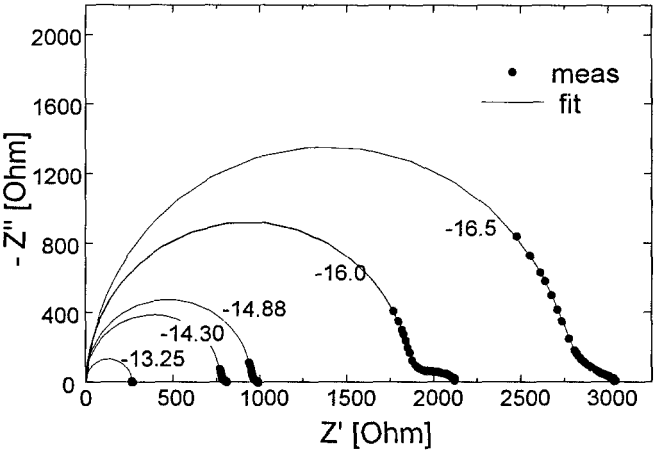

Fig. 7 Impedance spectra of polycrystalline fayalite as a function of oxygen fugacity, T=900°C

Effect of oxygen fugacity on the impedance spectra

New equilibrium was reached within 5 and 120 h after changing oxygen fugacity, depending on grain size. Figure 7 shows the effect of oxygen fugacity on the impedance spectra. As expected from Eq. (16), the spectra shift towards lower resistance with increasing oxygen fugacity, due to an increasing amount of electron holes associated with Fe^{3+} defects. Both bulk resistance and double layer resistance decrease with increasing oxygen fugacity. In addition, the portion of the bulk arc covered by the applied frequency range decreases with increasing oxygen fugacity.

Samples without coexisting SiO_2

A $\log f_{O_2} - \log R_{bulk}$ diagram (Fig. 8) shows a linear dependence of bulk resistance on oxygen fugacity. This behaviour is typical for all measured samples. The data plotted in Fig. 8 were measured on fayalite without a coexisting binary oxide. Therefore, according to Fig. 5,

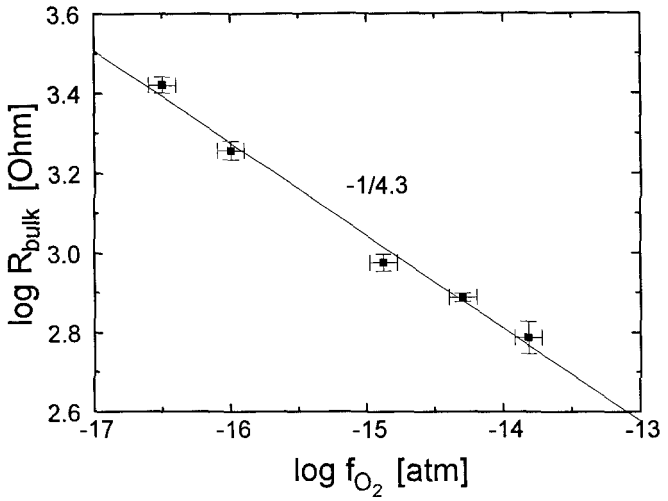

Fig. 8 Bulk resistance of polycrystalline fayalite as a function of oxygen fugacity, T=900°C

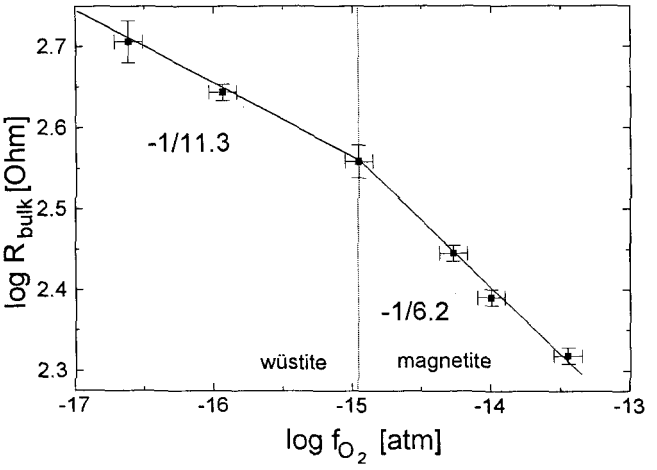

Fig. 9 Bulk resistance of polycrystalline fayalite coexisting with SiO_2 (i.e. $a_{SiO_2}=1$) as a function of oxygen fugacity, T=900°C

the slope should fall into the range from $-1/4.5$ to $-1/5$. The fitted slope is $-1/4.3$, which is in good agreement with the expected value.

Samples with coexisting SiO_2

Figure 9 shows the $\log f_{O_2}-\log R_{bulk}$ diagram of fayalite coexisting with SiO_2. According to Eq. (16), R_{bulk} should depend on the 6th root of oxygen fugacity. In Fig. 9, this is valid only at oxygen fugacities corresponding to the magnetite stability field (n=6.2). At the magnetite-wüstite boundary, the slope is lowered by a factor of about 2 to $-1/11.3$. The reason for this behaviour is not clear yet.

Several authors, e.g. Roberts and Tyburczy (1993), Constable and Duba (1990), observed a flattening of the conductivity-f_{O_2} curves under more reducing conditions in measurements of natural olivine. They fitted their data curves using the equation

$$\sigma=\sigma_0+\sigma_1\cdot f_{O_2}^{c} \tag{18}$$

where σ is the conductivity, σ_0 is conductivity independent of f_{O_2}, σ_1 is a preexponential term and c is the exponent of f_{O_2} (Constable and Duba 1990). Another model to fit their data could be based on the assumption that a principle change of conductivity occurs at the wüstite-magnetite (WM) boundary, with a linear dependence of conductivity below and above WM. The observed change of slope would be caused by the dominating point defect chemistry of the fayalite component in olivine.

Some samples showed a smaller f_{O_2}-dependence of bulk resistance than expected over the entire stability field, with and without coexisting SiO_2. Values varied between $-1/10$ and $-1/15$, i.e. the dependence is lowered by a factor of 2–3. Figure 10 is a typical example of a $\log R_{bulk}-\log f_{O_2}$ diagram showing these data. There are several possible explanations for the observed behaviour. Aliovalent impurities can have a major influence

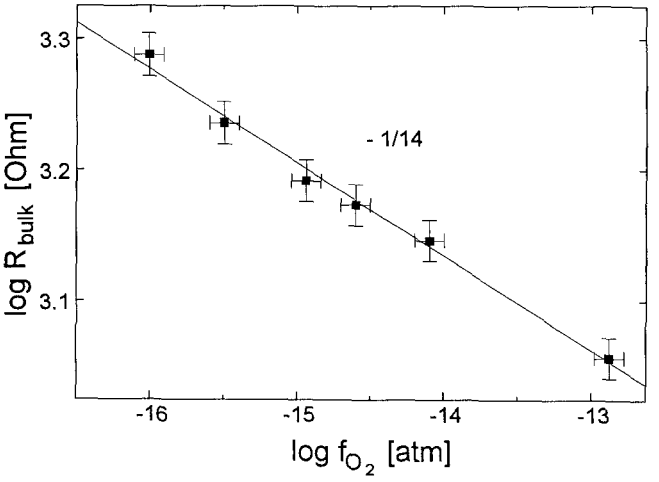

Fig. 10 Bulk resistance of polycrystalline fayalite as a function of oxygen fugacity, showing a lesser f_{O_2}-dependence than expected from the defect model, T=900°C

on the electroneutrality condition, as commonly accepted for alkaline earth titanates (e.g. Choi and Tuller 1988). The greater the (f_{O_2}-independent) concentration of electronic defects produced to balance the aliovalent impurities, the lower the contribution of electron holes produced by the majority defect reactions to the overall conductivity, and the lower the observed f_{O_2}-dependence of impedance or electrical conductivity, respectively.

The low f_{O_2}-dependence could also be caused, in theory, by self buffering effects due to additional phases in the sample, but there was no evidence found for such phases. Therefore, an explanation based on self buffering effects seems to be unlikely.

Polarization at the sample-electrode interface

Figures 11 a, b show the f_{O_2}-dependence of the low frequency arc. By variation of the sample geometry, this arc

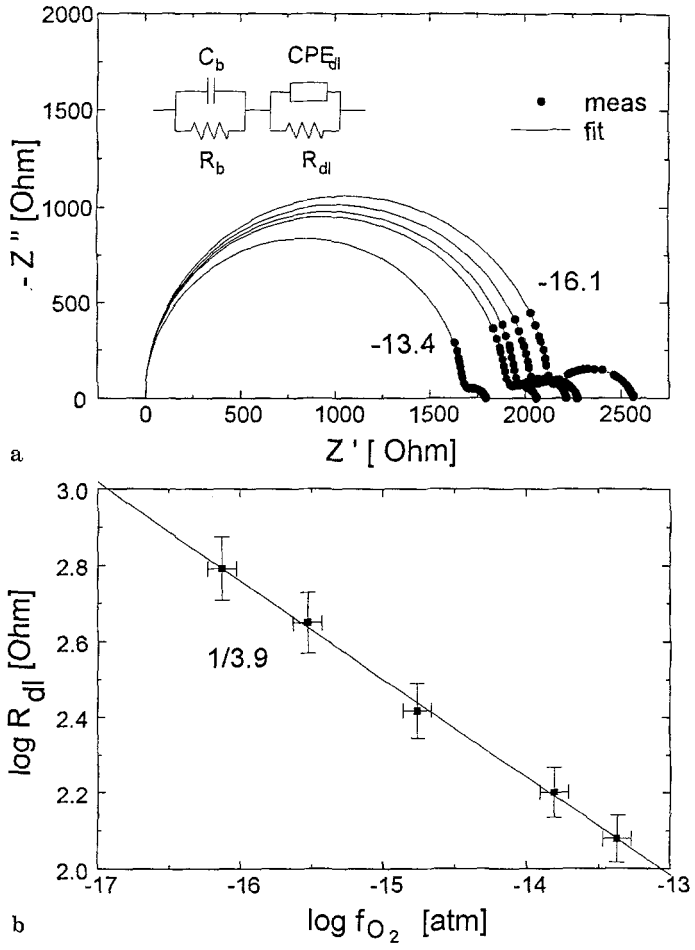

Fig. 11 **a** f_{O_2}-dependence of the polarization process at the sample-electrode interface (double layer), T=900°C; **b** Double layer resistance (R_{dl}) as a function of oxygen fugacity, T=900°C

was assigned to a polarization process at the sample-electrode interface. The electrode arc or double layer resistance, respectively, shows a much stronger f_{O_2}-dependence than the bulk resistance and is proportional to the $-1/2$ to $-1/4$ power of oxygen fugacity. This behaviour is interpreted as a reaction of the gas phase with the electrodes, as observed by Bauerle (1969) for ZrO_2, or Østergard and Mogensen (1993) for $La_{1-x}Sr_xMnO_3$.

Conclusions

The foregoing results show that impedance spectroscopy is an appropriate method to determine the electrical conductivity of polycrystalline material. In order to obtain bulk conductivities or resistances, all possible polarization processes in the system sample-electrode have to be taken into account. Pt is not suitable as an electrode material for measurements of iron bearing materials at high temperatures (i.e. >700°C) and reducing atmospheres (i.e. below QFM), because of a major iron-loss to the electrodes. The use of AgPd-electrodes is a possible alternative at temperatures below 1000°C, but there is still a critical need for a suitable, inert electrode material. The measured $\log f_{O_2} - \log R_{bulk}$ data can be fitted linearly. Some fayalite samples show a change of slope at oxygen fugacities corresponding to the wüstite-magnetite boundary. The flattening of σ-f_{O_2} curves, observed by several authors in the measurement of natural olivine, is possibly based on the same effect. This effect, which is not understood yet, might be connected to the point defect chemistry of the fayalite component. Finally, the effect of aliovalent impurities should be considered in the interpretation of electrical conductivity data of minerals, especially when natural samples are investigated.

Acknowledgement The authors gratefully acknowledge financial support by the Deutsche Forschungsgemeinschaft. We appreciate the helpful comments of the two anonymous reviewers.

References

Bauerle JE (1969) Study of solid electrolyte polarization by a complex admittance method. J Phys Chem Solids 30:2657–2670

Boukamp BA (1989) Equivalent circuit 3.96, Users Manual. University of Twente

Cemič L, Will G, Hinze E (1980) Electrical conductivity measurements on olivines Mg_2SiO_4–Fe_2SiO_4 under defined thermodynamic conditions. Phys Chem Minerals 6:95–107

Choi GM, Tuller HL (1988) Defect structure and electrical properties of single-crystal $Ba_{0.003}Sr_{0.97}TiO_3$. J Am Ceram Soc 71:201–205

Cole RH, Cole KS (1941) Dispersion and absorption in dielectrics: I. Alternating current characteristics. J Chem Phys 9:341–351

Constable SC, Duba AG (1990) The electrical conductivity of olivine, a dunite and the mantle. J Geophys Res 95:6967–6978

Huebner JS, Dillenburg RG (1995) Impedance spectra of hot, dry silicate minerals and rock: Qualitative interpretation of spectra. Am Mineral 80:46–64

Kröger FA, Vink HJ (1956) Relations between the concentrations of imperfections in crystalline solids. Solid State Phys 3:307–435

Macdonald JR (1987) Impedance Spectroscopy. John Wiley, New York

Nakamura A, Schmalzried H (1983) On the nonstoichiometry and point defects of olivine. Phys Chem Minerals 10:27–37

Nover G, Will G, Waitz R (1992) Pressure induced phase transition in Mg_2GeO_4 as determined by frequency dependent complex electrical resistivity measurements. Phys Chem Minerals 19:133–139

Østergard MJL, Mogensen M (1993) ac Impedance study of the oxygen reduction mechanism on $La_{1-x}Sr_xMnO_3$ in solid oxide fuel cells. Electrochim acta 38, 14:2015–2020

Roberts JJ, Tyburczy JA (1993) Frequency dependent electrical properties of dunite as functions of temperature and oxygen fugacity. Phys Chem Minerals 19:545–561

Schock RN, Duba AG, Shankland TJ (1989) Electrical conduction in olivine. J Geophys Res 94:5829–5839

Simons B (1986) Temperatur- und Druckabhängigkeit der Fehlstellenkonzentration der Olivine und Magnesiowüstite, Habilitationsschrift, Universität Kiel

Sockel HG (1974) Defect structure and electrical conductivity of crystalline ferrous silicate. In: Schmetzer MS and Jaffe RJ (ed) Defects and transport in oxides. Plenum Press, New York pp 341–355

Wanamaker BJ, Duba AG (1993) Electrical conductivity of San Carlos Olivine along [100] under oxygen- and pyroxene-buffered conditions and implications for defect equilibria. J Geophys Res 98:489–500